Inorg. Chem. **2003**, *42*, 6564–6574

Construction of Multiporphyrin Arrays Using Ruthenium and Rhodium Coordination to Phosphines

Eugen Stulz,*[,†,‡] Sonya M. Scott,[†] Yiu-Fai Ng,[†] Andrew D. Bond,[†,§] Simon J. Teat,[||] Scott L. Darling,[†] Neil Feeder,[†] and Jeremy K. M. Sanders*[,†]

University Chemical Laboratory, University of Cambridge, Lensfield Road, Cambridge, CB2 1EW, United Kingdom, and CLRC Daresbury Laboratory, Warrington, Cheshire, WA44AD, United Kingdom

Received June 19, 2003

The synthesis of linear multiporphyrin arrays with mono- and bisphosphine-substituted porphyrins as ligand donors and ruthenium(II) or rhodium(III) porphyrins as ligand acceptors is described. With appropriate amounts of the building blocks mixed, linear dimeric and trimeric arrays have been synthesized and analyzed by ^{1}H NMR and ^{31}P NMR spectroscopy. The Ru/Rh acceptor porphyrins can be located either at the periphery or in the center of the array. Likewise, the monophosphine porphyrins can be positioned at the periphery, thus allowing a high degree of freedom in the overall composition of the arrays. This way, both donor and acceptor porphyrins can act as chain extenders or terminators. One of the trimeric complexes with two nickel and one ruthenium porphyrin has also been analyzed by X-ray crystallography. Attempts have also been made to synthesize higher order arrays by mixing appropriate amounts of the porphyrins; however, from the NMR data it cannot be concluded if monodisperse five, seven, or nine porphyrin arrays are present or if the solutions are composed of a statistical mixture of smaller and larger arrays.

Introduction

The construction of multiporphyrin arrays, where the connectivity of the individual porphyrins is realized through central-metal coordination, has led to a number of linear,[1−3] branched,[4−6] cyclic,[7,8] dendritic,[9,10] and polymeric[11,12] assemblies. Despite the overall diversity of these assemblies, the individual constructs usually are homoporphyrinic in nature. Our concept of using simultaneous orthogonal metal−ligand coordination to synthesize mixed metallo-porphyrin arrays, first realized by the construction of a tin(IV)−zinc(II)−ruthenium(II) trimer,[13] has led to the synthesis of a heterometallic porphyrin undecamer combining Sn(IV)−oxygen and Rh(III)−nitrogen coordination and incorporating porphyrins in four different metalation states.[14] Recently, we have added the Ru(II)−phosphorus coordination linkage and demonstrated the utility of phosphine-substituted porphyrins to assemble linear dimeric and trimeric arrays.[15] With Ru(II) and Rh(III) porphyrins, cyclic tetraporphyrin arrays

* Authors to whom correspondence should be addressed. E-mail: eugen.stulz@unibas.ch (E.S.); jkms@cam.ac.uk (J.K.M.S.).

† University of Cambridge.

‡ Present address: Department of Chemistry, University of Basel, St. Johanns-Ring 19, 4056 Basel, Switzerland.

§ Present address: Syddansk Universitet, Kemisk Institut, Campusvej 55, 5230 Odense M, Denmark.

|| CLRC Daresbury Laboratory.

(1) Funatsu, K.; Kimura, A.; Imamura, T.; Ichimura, A.; Sasaki, Y. *Inorg. Chem.* **1997**, *36*, 1625−1635.
(2) Maiya, B. G.; Bampos, N.; Kumar, A. A.; Feeder, N.; Sanders, J. K. M. *New J. Chem.* **2001**, *25*, 797−800.
(3) Mak, C. C.; Bampos, N.; Darling, S. L.; Montalti, M.; Prodi, L.; Sanders, J. K. M. *J. Org. Chem.* **2001**, *66*, 4476−4486.
(4) Mak, C. C.; Bampos, N.; Sanders, J. K. M. *Chem. Commun.* **1999**, 1085−1086.
(5) Susumu, K.; Tanaka, K.; Shimidzu, T.; Takeuchi, Y.; Segawa, H. *J. Chem. Soc., Perkin Trans. 2* **1999**, 1521−1529.
(6) Giribabu, L.; Rao, T. A.; Maiya, B. G. *Inorg. Chem.* **1999**, *38*, 4971−4980.
(7) Ambroise, A.; Li, J. Z.; Yu, L. H.; Lindsey, J. S. *Org. Lett.* **2000**, *2*, 2563−2566.
(8) Haycock, R. A.; Hunter, C. A.; James, D. A.; Michelsen, U.; Sutton, L. R. *Org. Lett.* **2000**, *2*, 2435−2438.
(9) Prodi, A.; Indelli, M. T.; Kleverlaan, C. J.; Scandola, F.; Alessio, E.; Gianferrara, T.; Marzilli, L. G. *Chem.−Eur. J.* **1999**, *5*, 2668−2679.
(10) Darling, S. L.; Mak, C. C.; Bampos, N.; Feeder, N.; Teat, S. J.; Sanders, J. K. M. *New J. Chem.* **1999**, *23*, 359−364.
(11) Michelsen, U.; Hunter, C. A. *Angew. Chem., Int. Ed.* **2000**, *39*, 764+.
(12) Imamura, T.; Fukushima, K. *Coord. Chem. Rev.* **2000**, *198*, 133−156.
(13) Kim, H. J.; Bampos, N.; Sanders, J. K. M. *J. Am. Chem. Soc.* **1999**, *121*, 8120−8121.
(14) Redman, J. E.; Feeder, N.; Teat, S. J.; Sanders, J. K. M. *Inorg. Chem.* **2001**, *40*, 2486−2499.
(15) Darling, S. L.; Stulz, E.; Feeder, N.; Bampos, N.; Sanders, J. K. M. *New J. Chem.* **2000**, *24*, 261−264.

10.1021/ic034699w CCC: $25.00 © 2003 American Chemical Society
Published on Web 09/11/2003

Scheme 1 [a]

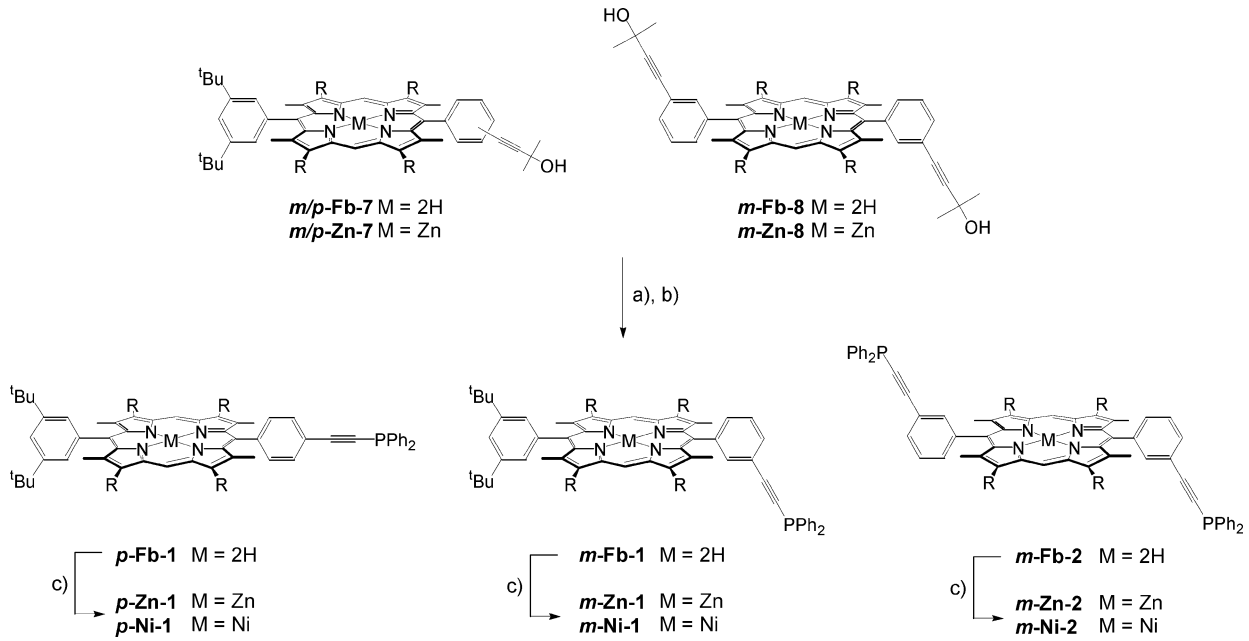

[a] Reagents and conditions: (a) NaOH, PhMe−^{n}BuOH, reflux, 5 h, 95%; (b) LiHMDS, $CdCl_2$ $ClPPh_2$, THF, −78 °C to RT, 60%; and (c) $Zn(OAc)_2$ or $Ni(OAc)_2$, $CHCl_3$−MeOH, reflux; quantitative. R = C_6H_{13}.

Chart 1

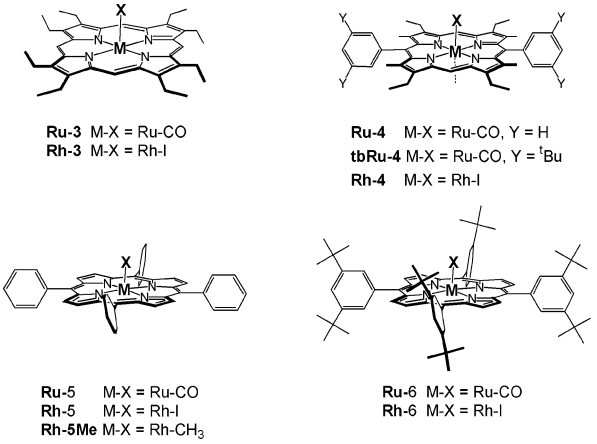

have been selected and amplified virtually completely from a biased dynamic combinatorial library using 4,4′-bipyridine as scaffold, the cyclic complex being stabilized by orthogonal Ru(II)− or Rh(III)−phosphorus and Zn(II)−nitrogen coordination.[16] Here, we report on the use of mono- and bisphosphine-substituted porphyrins ***m*-1**, ***p*-1**, and ***m*-2** (Scheme 1) as ligand donors (**D**) and their coordination behavior toward a variety of Ru(II) and Rh(III) porphyrins (Chart 1) as ligand acceptors (**A**). The approach used here to construct arrays incorporating porphyrins displaying a large diversity in substitution pattern and central metal expands the diversity in previously synthesized arrays.

The synthesis of acetylenic phosphines is well documented,[17,18] and they provide easily accessible and versatile ligands for both ruthenium and rhodium porphyrins.[19−21] Since they are sterically much less demanding than their triaryl counterparts, their complexes with acceptor porphyrins show enhanced stability. Our previous investigations on the properties of ruthenium complexes with a series of phenyl acetylene phosphines and phosphonites as model complexes for the arrays discussed below have shown that the electronic properties of the acceptor porphyrins are largely unaffected by the substitution pattern on the acetylene phosphorus ligand.[19,20] Thus, we have focused on the diphenyl substitution pattern on the phosphine, which conveniently is also the most straightforward derivative to synthesize (Scheme 1).

Monophosphine complexes of the form P−Ru(CO)(por) (por = porphyrin) are stable in solution, but partial decarbonylation occurs upon isolation of the complexes, leading to the bisphosphine ruthenium complexes P_2−Ru(por).[19,20] Isolation of arrays containing monocoordinated ruthenium(II) porphyrins is therefore not expected. Rhodium(III) porphyrins also provide access to the bisphosphine complexes P_2−Rh(por),[21] since the iodide on the rhodium is readily displaced in solution (in P−Ru(CO)(por), complete removal of the carbonyl ligand must be achieved by repeated evaporating−dissolving cycles). In contrast, the σ-bonded methyl group in Rh(Me)(por) is inert to displacement by DPAP, giving easy access to monophosphine rhodium complexes P−Rh(Me)(por) with essentially the same electronic properties as for P_2−Rh(por) complexes.

(16) Stulz, E.; Ng, Y. F.; Scott, S. M.; Sanders, J. K. M. *Chem. Commun.* **2002**, 524−525.
(17) Carty, A. J.; Hota, N. K.; Ng, T. W.; Patel, H. A.; O'Connor, T. J. *Can. J. Chem.* **1971**, *49*, 2706−2711.
(18) Hengefeld, A.; Kopf, J.; Rehder, D. *Organometallics* **1983**, *2*, 114−121.
(19) Stulz, E.; Maue, M.; Feeder, N.; Teat, S. J.; Ng, Y. F.; Bond, A. D.; Darling, S.; Sanders, J. K. M. *Inorg. Chem.* **2002**, *41*, 5255−5268.
(20) Stulz, E.; Sanders, J. K. M.; Montalti, M.; Prodi, L.; Zaccheroni, N.; de Biani, F.; Grigiotti, E.; Zanello, P. *Inorg. Chem.* **2002**, *41*, 5269−5275.
(21) Stulz, E.; Scott, S. M.; Bond, A. D.; Otto, S.; Sanders, J. K. M. *Inorg. Chem.* **2003**, *42*, 3086−3096.

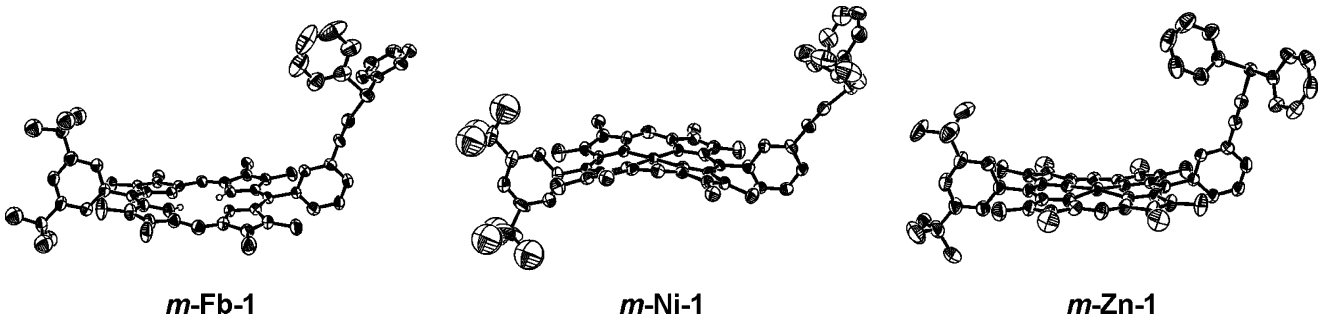

Figure 1. Molecular units of ***m*-Fb-1**, ***m*-Ni-1**, and ***m*-Zn-1**, showing atomic displacement ellipsoids drawn at the 50% probability level. Hydrogen atoms and the hexyl side chains (except for the first carbon atom) have been omitted for clarity.

The series of acceptor porphyrins (Chart 1) has been chosen with the aim of incorporating a large structural diversity into the arrays, varying both in the central metal and in the substitution pattern. The latter is based on an increasing number of *meso*-phenyl substituents on the porphyrin, ranging from none in **Ru/Rh-3** (octaethyl porphyrin, OEP) to two in **Ru/Rh-4** (5,15-diphenyl porphyrin, DEDPP) and four in **Ru/Rh-5** (tetraphenyl porphyrin, TPP). In this respect, **Ru/Rh-4** may be considered as a structural hybrid between TPP and OEP. The 3′,5′-di-^{t}Bu derivatives **tbRu-4** and **Ru/Rh-6** were chosen to probe the steric influence on the stability of the arrays, and **Rh-5Me** should be useful to form selective monophosphine complexes with a rhodium porphyrin. From our studies with DPAP,[19−21] we can expect that the association constants in solution of the phosphine-substituted porphyrins to the acceptor porphyrins to be within the range of 10^6 M^{-1} for mono- and bisphosphine complexes with ruthenium porphyrins, 10^4 M^{-1} for bisphosphine complexes with rhodium porphyrins, and 10^4 M^{-1} in the case of complexes with **Rh-5Me**.

Here we demonstrate that the phosphine porphyrin building blocks ***m*-1**, ***p*-1**, and ***m*-2** either can be used to form homopolymeric supramolecular structures in the solid state or can be incorporated into discrete linear dimeric, trimeric, pentameric, heptameric, and nonameric heteroporphyrinic arrays. The arrays, which are thermodynamically stable at ambient temperature and millimolar concentration, were characterized by ^{1}H, ^{31}P{^{1}H}, and 2D-NMR spectroscopy. In the linear arrays, ***m*-2** and **Ru/Rh-3−6** act as chain extenders, whereas ***m*/*p*-1**, Ru(CO)(por), and **Rh-5Me** can be used to terminate the chain. The ratio of extender vs terminator determines the length of the chain obtained.

Results and Discussion

Synthesis and Characterization of the Phosphine-Substituted Porphyrins. The synthetic route to acetylenic diphenyl phosphine substituted porphyrins is outlined in Scheme 1 (full experimental details are available as electronic Supporting Information (SI)). The tertiary hydroxy protecting group for the acetylene substituent has a major advantage over the use of the TMS protecting group in the mixed porphyrin synthesis in that the products can be separated with greater ease by column chromatography due to their distinctively different polarity. Deprotection of the acetylene by base is best performed on the zinc(II)-metalated porphyrins **Zn-7** and **Zn-8**, respectively. Attachment of the diphenyl phosphine group via a cadmium(II) Grignard-type reaction yields the diphenyl phosphine porphyrins ***p*-1**, ***m*-1**, and ***m*-2**. The synthesis and characterization of the porphyrins ***m*-1** and ***p*-1** have been described earlier,[15] but the data for ***m*-2** and the porphyrins **7** and **8** are given for the first time. The characteristic ^{1}H NMR chemical shifts of the meso protons of the porphyrins are independent of the substitution pattern on the *meso*-phenyl substituents. The ^{31}P{^{1}H} NMR spectra show the typical resonance for the acetylene phosphine at $\delta(^{31}P) = -32$ ppm, which is independent both of the metalation state and of the substitution pattern of the porphyrin and is isochronous with the resonance of the model ligand DPAP. These data indicate that there is no electronic communication between the phosphine substituents and the porphyrin core.

The synthesis, workup, and purification of the porphyrins must be carried out with strict exclusion of oxygen, since the phosphines are highly susceptible to oxidation. The formation of the phosphine oxide can be followed by ^{31}P NMR spectroscopy, showing a characteristic resonance at δ 9 ppm for all mono- and diphosphine oxides. In the case of ***p*-Zn-1**, formation of the phosphine oxide has also been confirmed by single-crystal X-ray diffraction analysis.[22] In contrast to the synthesis of the building block ***m*-2**, the formation of the para-substituted diphosphine porphyrin was not clean due to the low solubility of the intermediate dilithiated bisacetylene and the increased sensitivity of the para isomer to oxidation. We therefore did not pursue the *p*-diphosphine building blocks any further.

Crystal Structures of the *m*-Monophosphine Porphyrins. We have reported previously the crystal structure of ***p*-Zn-1**.[15] In this paper, we present the single-crystal structures of the *m*-monophosphines ***m*-Fb-1**, ***m*-Zn-1**, and ***m*-Ni-1** (Figure 1). Selected geometrical data are compiled in Table 1. The crystallographic data are given in the electronic SI. Crystals of ***m*-Fb-1** were small and weakly diffracting, and a synchrotron radiation source was utilized to collect diffraction data for this compound.[23] In all three structures, several of the hexyl substituents were found to be disordered and these were modeled in two orientations with restrained geometries. A single isotropic displacement parameter was refined for each hexyl chain, scaled along

(22) Darling, S. L.; Sanders, J. K. M.; Feeder, N. Private communication to the CCDC, 1999. CSD Refcode: HOJCOY.

Table 1. Selected Geometrical Data for ***m*-Fb-1**, ***m*-Zn-1**, and ***m*-Ni-1**

	m-Fb-1	*m*-Zn-1	*m*-Ni-1
Zn/Ni−N1/Å		2.062(5)	1.937(9)
Zn/Ni−N2/Å		2.051(4)	1.923(9)
Zn/Ni−N3/Å		2.080(5)	1.948(9)
Zn/Ni−N4/Å		2.051(5)	1.955(8)
σ/Å	0.177	0.107	0.270
δ/°[a]	80.3(1) (C5−Ph)	80.5(1) (C5−Ph)	81.4(2) (C5−Ph)
	75.8(1) (C15−Ph)	87.8(2) (C15−Ph)	83.8(3) (C15−Ph)
d/Å	0.192(5) (C5)	0.201(5) (C5)	0.283(10) (C5)
	−0.192(6) (C10)	−0.062(6) (C10)	−0.498(11) (C10)
	0.205(5) (C15)	0.118(5) (C15)	0.526(11) (C15)
	−0.138(5) (C20)	−0.208(5) (C20)	−0.433(12) (C20)

[a] C5 is substituted with the phenyl ring bearing the acetylene phosphine group.

the length of the chain, such that the first carbon atom has $U_{iso} = 1 \times$ free variable, the second carbon atom has $U_{iso} = 1.15 \times$ free variable, etc. All porphyrins adopt a ruffle distortion, in which the meso carbons around the core are displaced alternately upward and downward with respect to the mean porphyrin plane (expressed by the deviation (*d*) perpendicular to the porphyrin plane in Table 1). The absolute deviation from planarity (measured by the average perpendicular deviation from the least-squares plane through all 24 porphyrin core atoms, denoted σ in Table 1) is specific to the metalation state; the average deviations in ***m*-Fb-1** ($\sigma = 0.177$ Å) and ***m*-Zn-1** ($\sigma = 0.107$ Å) are similar and are much smaller than those in ***m*-Ni-1** ($\sigma = 0.270$ Å). The large distortion in the latter stems from the relatively small size of the nickel(II) ion (reflected by the relatively short Ni−N bond distances) and its tendency to drive the ideal square-planar geometry of the porphyrin toward the preferred tetrahedral geometry; the geometry in ***m*-Ni-1** is not unusual for electronically unperturbed nickel(II) porphyrins. In all three structures, the *meso*-phenyl substituent to which the phosphine group is attached is rotated with respect to the porphyrin plane by an angle in the range 75−88° (expressed as the dihedral angle δ between the least-squares planes of the phenyl ring and the porphyrin core, Table 1). The phenyl groups of the phosphine point inward toward the porphyrin, such that the lone pair of the phosphorus points away from the porphyrin. Slight variations in the relative orientation of the phosphine group are observed in the three structures, consistent with observed rotational freedom around the acetylene spacer (indicated by the equivalency of the corresponding phenyl protons in the solution ^{1}H NMR spectra). The exact conformational preference of the phosphine group in the three structures is likely to be influenced by secondary intermolecular interactions.

***m*-Fb-1** crystallizes in space group $P2_1/n$ as monomeric units that associate across centers of symmetry, adopting coplanar arrangements with a perpendicular separation of 3.55(1) Å between least-squares planes. The lateral offset between adjacent porphyrins is large (centroid−centroid separation 8.00(2) Å), however, so that the interaction does not constitute significant $\pi-\pi$ stacking. Adjacent dimers also associate in coplanar arrangements but with a somewhat larger interplanar separation (3.86(1) Å) and a centroid−centroid separation of 8.96(2) Å. Thus, offset stacks are formed with alternate large and small interporphyrin separations. Between these stacks, hexyl chains interlock and the phosphine substituents associate such that the edge of the *meso*-phenyl group bearing the phosphine fits into the concave surface formed by the two phenyl rings of an adjacent phosphine group. The lone pair of the phosphorus atom is directed toward a hydrogen atom of the *meso*-phenyl group in the 10-position of an adjacent porphyrin, with an H···P separation of 3.28 Å and a C−H···P angle of 138.0 Å, and does not appear to have any significant structure-directing role.

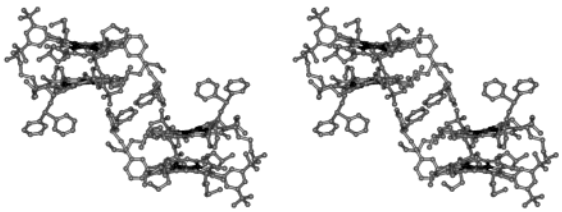

Figure 2. Stereo representation of part of the crystal packing in ***m*-Ni-1**. Hydrogen atoms are omitted for clarity.

In the crystal structure of ***m*-Ni-1** (space group $P2_1/c$), porphyrins adopt offset $\pi-\pi$ stacking arrangements with a separation of 3.73(1) Å between the least-squares planes of adjacent porphyrins and a Ni···Ni offset distance of 6.554(1) Å. Alternate porphyrins within a single stack are rotated by ca. 120° with respect to each other, facilitating effective matching of the distorted porphyrin cores (Figure 2). The stacks may be considered to form layers parallel to the crystallographic *bc* plane, with the alkyl and *tert*-butylphenyl substituents interlocking between adjacent stacks within each layer. The layers expose predominantly alkyl and *tert*-butylphenyl substituents on one side and alkyne phosphine substituents on the other side, which associate like-to-like; the phenyl groups of the alkyne phosphine substituents associate in mutual edge−face arrangements across centers of symmetry (forming a quadruple "phenyl embrace"),[24] and the alkyl and *tert*-butylphenyl substituents interlock on the opposite side of the layers, leading to an overall bilayer-type arrangement.

Clearly, there is no intermolecular coordination between the phosphine and the Ni centers of adjacent porphyrins in ***m*-Ni-1**. By contrast, intermolecular coordination of the phosphine to the zinc atom is observed in the crystal structure of ***m*-Zn-1**. This is consistent with the solution NMR spectrum of ***m*-Zn-1** (and also ***p*-Zn-1**), which displays a broadened ^{31}P{^{1}H} NMR resonance, which sharpens upon cooling the sample to −20° or upon addition of pyridine.[15]

(23) In the refined structure of ***m*-Fb-1**, residual electron density of ca. 3.0 e Å^{-3} was observed at the center of the porphyrin cavity. This result was repeated for several different crystals and was interpreted therefore as a partial zinc atom, present in ca. 8% of the porphyrin molecules, probably as a result of incomplete demetalation during acidic workup in this particular sample. It should be noted that the structure of ***m*-Fb-1** differs dramatically from that of ***m*-Zn-1** (reported herein), and we conclude therefore that the gross structure is that of the free-base form. Literal interpretation of the X-ray results would suggest that the crystals analyzed actually comprise solid solutions of ca. 8% ***m*-Zn-1** in a lattice of ***m*-Fb-1**.

(24) Dance, I.; Scudder, M. *J. Chem. Soc., Chem. Commun.* **1995**, 1039−1040.

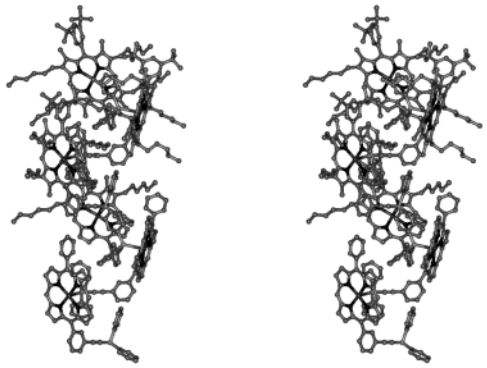

Figure 3. Stereo representation of the helical structure in the crystal of ***m*-Zn-1**. In the lower part, the hexyl side chains on the porphyrins and the ^{t}Bu groups on the *meso*-phenyl substituents have been omitted to allow better view of the interior of the helix.

This behavior is indicative of weak binding of the phosphine to the zinc porphyrin and is not observed in the free-base or nickel analogues. The zinc−phosphorus bond distance of 2.792(2) Å in ***m*-Zn-1** is relatively long compared with the metal−phosphorus bond distances of 2.3−2.4 Å found in ruthenium or rhodium porphyrin complexes and suggests that the interaction is rather weak not only in solution but also in the solid state.

Compared with ***p*-Zn-1**, which forms a dimeric methanol complex in the solid state,[15] the shift of the acetylene substituent from the para to the meta position has a dramatic impact on the intermolecular association. In ***m*-Zn-1**, Zn−P coordination leads to formation of a C_3-symmetrical helix, with a helical repeat distance of ca. 18 Å (the lattice parameter *c*, Figure 3). In the crystal, the helices are arranged into a hexagonal superstructure in which right-handed and left-handed helices are always adjacent to each other (rendering the overall crystal structure achiral, Figure 4).The internal part of each helix is largely occupied by the phenyl substituents on the phosphorus, which show mutual edge−face interactions. Between helices, porphyrins adopt offset $\pi-\pi$ stacking arrangements, with a distance of 3.63(1) Å between the least-squares planes of adjacent porphyrins and a Zn···Zn offset separation of 5.170(1) Å. This arrangement of helices leaves apparent tubular channels, which are filled by (disordered) hexyl side chains. Two hexyl side chains that are part of the same unsubstituted dipyrromethane moiety (i.e., at the 7- and 13-positions of the macrocycle core) interlock within the channels, while the other two wrap partially around the helices to form an apparent hydrophobic surface (Figure 3 and Figure 4).

Two-Porphyrin Arrays. In a previous report, we have shown that ***m*-1** and ***p*-1** readily form two-porphyrin dimeric arrays with **tbRu-4** both in solution and in the gas phase, the latter being analyzed by matrix-assisted laser desorption ionization time-of-flight mass spectrometry.[15] This can be generalized to all ruthenium porphyrins investigated here, including the sterically hindered **Ru-6**. In Figure 5, the low-field region of the ^{1}H NMR spectra of the OEP-complexes **[*m*-Fb-1/Ru-3]** and **[*p*-Fb-1/Ru-3]** and of the complexes with the bulky TPP-derivative **[*p*-Fb-1/Ru-6]** and **[*m*-Fb-1/Ru-6]** are shown. The dimeric complexes show two sets of signals of nonequal integral values in the ^{1}H NMR spectra for both porphyrins, one set consisting of sharp resonances (H_x in Figure 5) and the other consisting of slightly broadened resonances (H_x' in Figure 5). This aspect is most predominant for the *meso*- and β-pyrrole protons of the porphyrins (δ 8.5−10.5, denoted $H_{m(1)}$, H_b and $H_{m(3)}$ in Figure 5) and for the ortho protons of the phenyl substituent of the bound phosphine ($\delta \sim 4.5$ ppm, denoted H_o). This feature also extends to the signals of the pyrrole nitrogen protons at

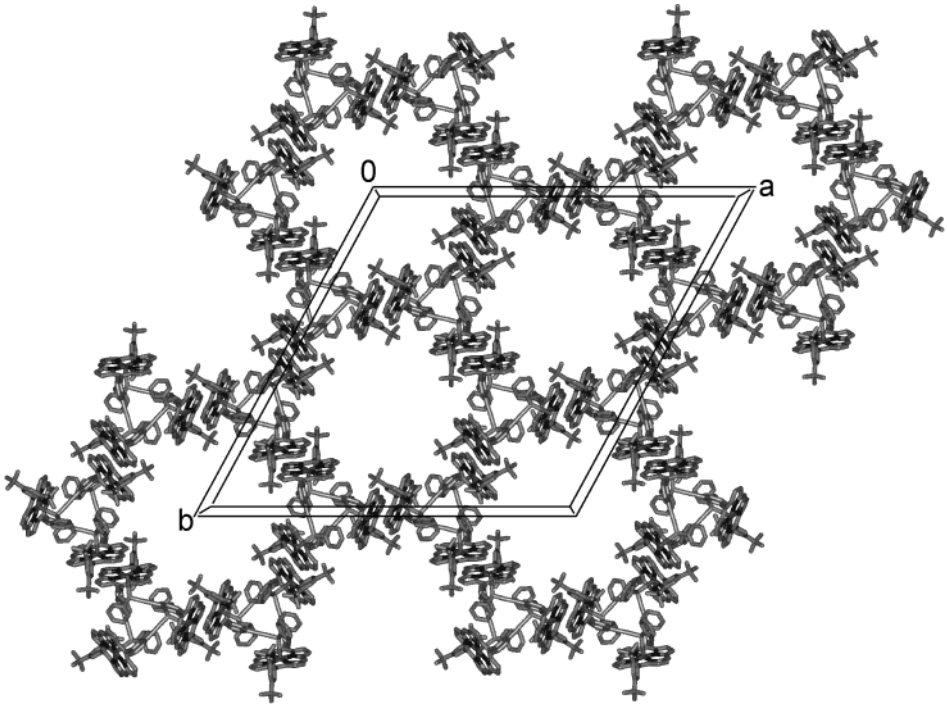

Figure 4. Crystal packing diagram in ***m*-Zn-1**, viewing along the crystallographic *c*-axis. The hexyl side chains on the porphyrins and the hydrogens have been omitted.

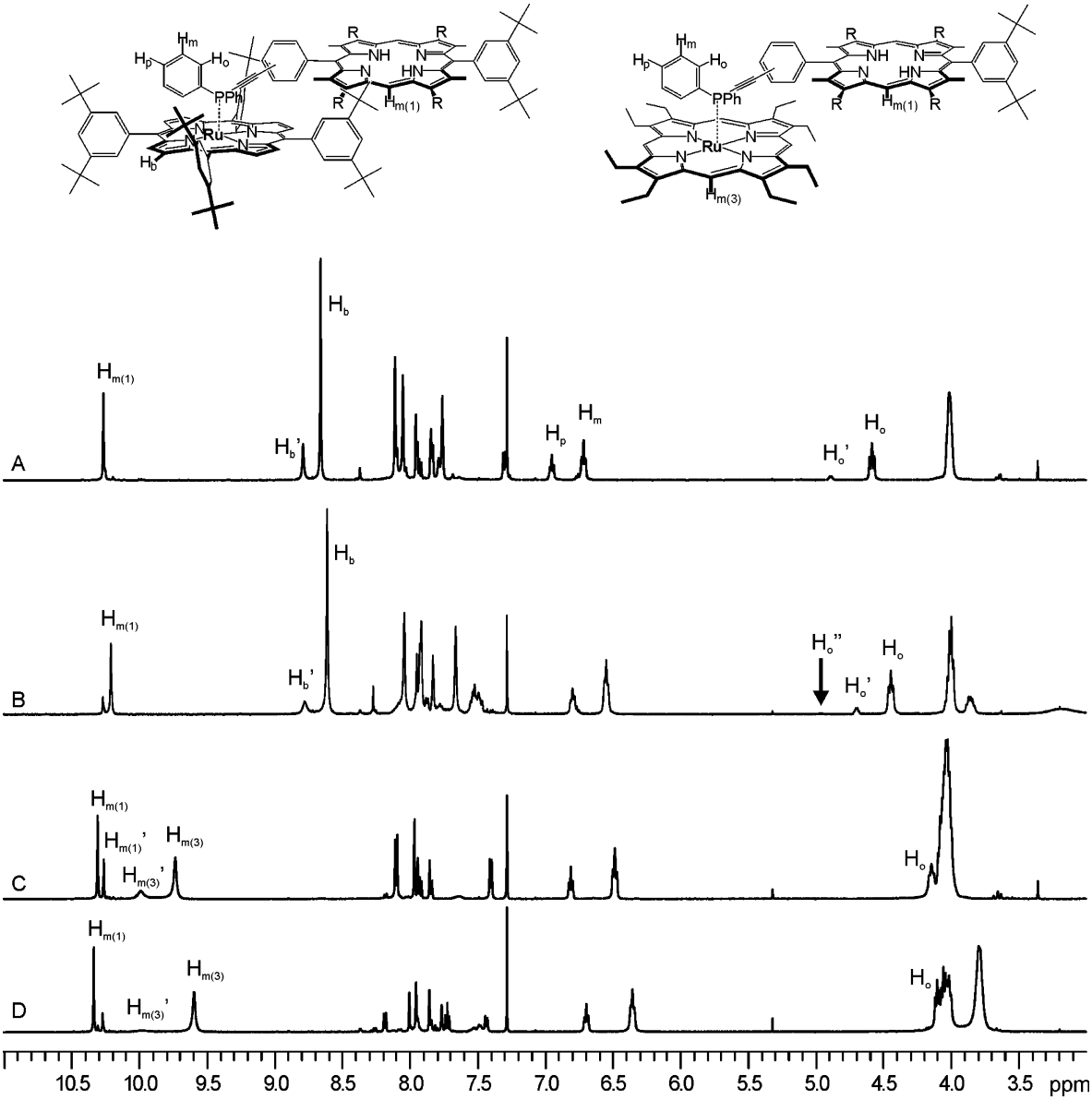

Figure 5. Low-field region of the ^{1}H NMR spectra of (A) **[*p*-Fb-1/Ru-6]**, (B) **[*m*-Fb-1/Ru-6]**, (C) **[*p*-Fb-1/Ru-3]**, and (D) **[*m*-Fb-1/Ru-3]**.

$\delta \sim -2.5$ ppm (not shown). In the ^{1}H NMR spectrum of **[*m*-Fb-1/Ru-6]**, an additional very weak signal at δ 4.70 ppm (H_o'') could be identified and assigned to a third conformation from the ^{1}H−^{1}H nuclear Overhauser effect spectrometry (NOESY) spectrum (dash-dotted lines in Figure 6). Since the ^{31}P NMR spectra showed only bound phosphine (δ −12 ppm, singlet resonance), there is no equilibrium between free and bound species, and the splitting of the signals must arise from two distinct conformations, which are stable on the chemical-shift time scale. Studies with CPK models suggest that rotation around the acetylene group could result in two different conformations, and cross-peaks in the ^{1}H−^{1}H NOESY spectra between the two sets of signals indicate that these are slowly interchanging at room temperature. Figure 6 shows part of the ^{1}H−^{1}H NOESY spectrum of **[*m*-Fb-1/Ru-6]**. NOE connectivities between H_b and the hexyl side chain of ***m*-Fb-1** and between H_a and H_c prove the integrity of the complex, and the cross-peaks between the resonances of the bound ligand H_o, H_o', and H_o'' show the interconversion of the different conformations. The relative ratio of the two different conformations is 1:0.5 in **[*p*-Fb-1/Ru-3]**, 1:0.3 in **[*p*-Fb-1/Ru-6]**, 1:0.2 in **[*m*-Fb-1/Ru-3]**, and 1:0.1 in **[*m*-Fb-1/Ru-6]**. The smaller integral values always correspond to the broadened set of resonances. The resonances H_b' and $H_{m(3)}'$ become smaller, broader, and more downfield shifted when the ligand is changed from ***p*-Fb-1** to ***m*-Fb-1**, which could indicate reduced stability of the conformation associated with these signals. At present, the exact geometries of the two conformations are not clear. It seems that two major conformations are present but probably more could be possible in the case of **[*m*-Fb-1/Ru-6]**. In the analogous complexes with the model ligand DPAP, only one averaged spectrum per ruthenium complex could be observed.[19,20]

As expected,[21] dimeric complexes with the iodo rhodium porphyrins were not formed cleanly, except with **Rh-5Me**, as shown in Figure 7 for the **[*m*-Fb-1/Rh-5Me]** complex. In this case, splitting of the proton resonances was not observed, but the ^{31}P NMR spectrum showed a slightly

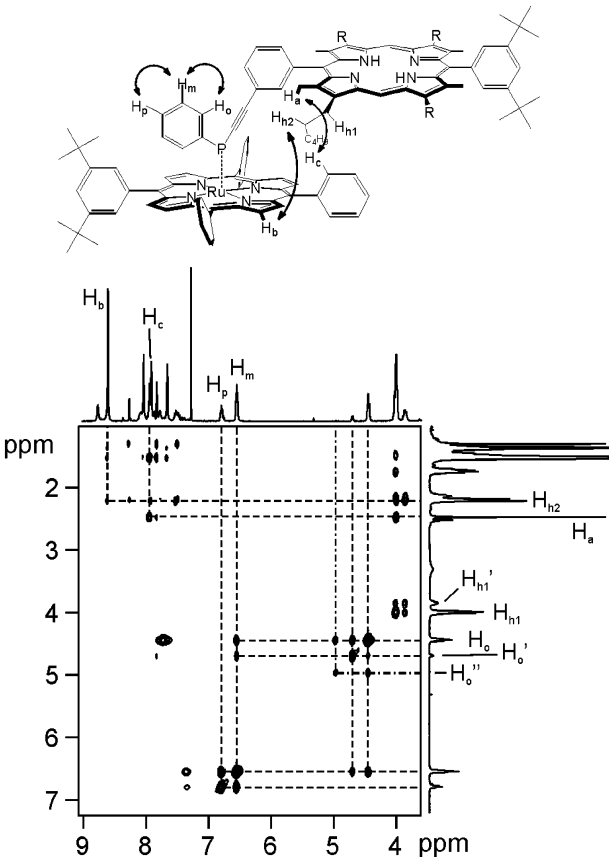

Figure 6. Part of the NOESY spectrum of **[*m*-Fb-1/Ru-6]**.

broadened resonance at δ −28 ppm for the bound phosphine, analogous to the DPAP−**Rh-5Me** complex. The diagnostic proton resonances are highlighted; the singlets at δ 10.26 ppm (meso proton of ***m*-Fb-1**) and 8.69 ppm (β-pyrrole proton of **Rh-5Me**) confirm the 1:1 stoichiometry, the upfield shifted resonances of the phenyl substituents of the phosphine at δ 6.93 ppm (para), 6.70 ppm (meta), and 4.72 ppm (ortho) confirm binding of the phosphine in the shielding region of **Rh-5Me**, and the resonance at the very low value of δ −6.27 ppm (σ-bonded methyl group on **Rh-5Me**) is consistent with monomeric binding of phosphine to rhodium.

Complexes with the various donor and acceptor porphyrins are possible in all combinations (except for rhodium) by mixing equimolar amounts of the donor and acceptor porphyrins, leading to stable dimeric arrays of the form **A**−**D**. In the ruthenium(II) arrays, different conformers could be detected by ^{1}H NMR spectroscopy. On the other hand, the rhodium(III) arrays having an association constant that is about 100 times smaller than those in the Ru(II) complexes, the larger off-rate leads to a shorter lifetime of one particular conformer; hence only an averaged proton NMR spectrum is observed. The crystal structures of the model complexes with DPAP reveal that the complex with **Rh-5Me** has a Rh−P bond distance (2.512(3) Å) significantly longer than the typical Ru−P bond distance (ca. 2.36 Å), and the binding constant is also lower by a factor of about 10^3. These properties might allow for several possible conformations of the rhodium complex to interconvert rapidly on the NMR time scale.

Three-Porphyrin Arrays. Three-porphyrin arrays are readily available from 2:1 mixtures of donor−acceptor porphyrins.[15] All of the ruthenium porphyrins investigated

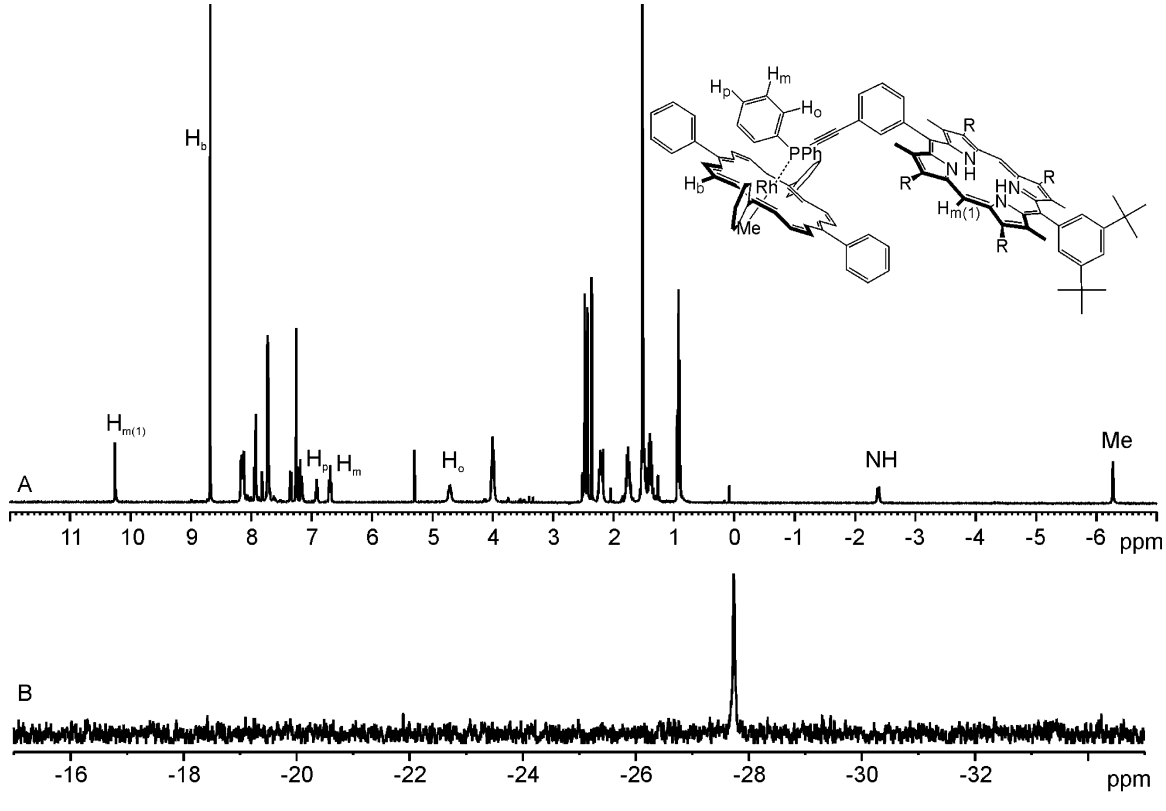

Figure 7. (A) ^{1}H NMR and (B) ^{31}P NMR spectra of **[*m*-Fb-1/Rh-5Me]**.

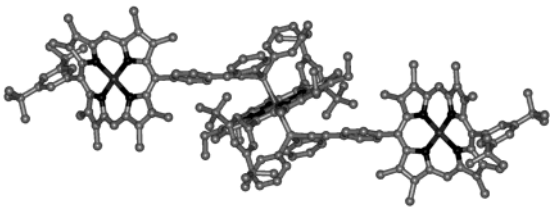

Figure 8. X-ray structure of **[*p*-Ni-1/tbRu-4/*p*-Ni-1]**. Hydrogen atoms and the hexyl side chains (except for the first carbon atom) have been omitted for clarity.

Table 2. Selected Geometrical Parameters for **[*p*-Ni-1/tbRu-4/*p*-Ni-1]**

	***p*-Ni-1** residue	**tbRu-4** residue
Ni/Ru−N1/Å	1.915(8)	2.067(6)
Ni/Ru−N2/Å	1.924(8)	2.075(6)
Ni/Ru−N3/Å	1.920(8)	
Ni/Ru−N4/Å	1.939(8)	
σ /Å	0.470	0.046
δ/° [a]	69.9(2) (C5−Ph) 66.4(2) (C15−Ph)	85.8(2) (C5/15-Ph)
d/Å	0.473(9) (C5) −0.482(11) (C10) 0.497(10) (C15) −0.504(12) (C20)	0.083(8) (C5) −0.011(7) (C10)
Ru−P/Å	2.343(2)	
α/° [b]	86.2(1)	

[a] C5 is substituted with the phenyl ring bearing the acetylene phosphine group. [b] α denotes the angle between the ruthenium−phosphorus bond and the least-squares plane of the porphyrin core of **tbRu-4**.

here form bisphosphine complexes in the same way. Thus, the diphenyl porphyrin−acetylene substitution pattern on the ligand does not interfere with the coordination abilities of the phosphine, and formation of stable trimeric arrays is unaffected by employing sterically hindered ruthenium porphyrins such as **Ru-6**. The $^{31}P\{^1H\}$ NMR spectra show singlet resonances in the range of δ −1 ppm (**Ru-3**) to +3 ppm (**Ru-6**), consistent with the chemical shift of bisphosphine ruthenium porphyrin complexes.[19] In the ^1H NMR spectra, further splitting of the signals is observed as compared to the dimeric arrays. For example, in **[*m*-Fb-1/Ru-6/*m*-Fb-1]**, the β-pyrrole protons of **Ru-6** appear as three singlets at δ 8.24, 8.17, and 8.15 ppm in a ratio of 0.1:1:0.8 (the spectra of all the arrays discussed here can be found in the electronic SI). The extension of the array from two to three porphyrins thus also increases the complexity of the constructs in solution.

The trimeric array **[*p*-Ni-1/tbRu-4/*p*-Ni-1]** was crystallized from a chloroform solution layered with methanol, giving small, weakly diffracting single crystals that were examined using a synchrotron radiation source. The molecular unit of the array is shown in Figure 8, and selected geometrical parameters are given in Table 2. The complex crystallizes as a dichloroform solvate in space group $P\bar{1}$, with the ruthenium atom sited on a center of symmetry. The nickel−porphyrin units show a ruffle distortion similar to that in ***m*-Ni-1** but deviating much further from planarity (σ 0.470 Å). This is also expressed in the larger deviation of the meso carbons (*d*) perpendicular to the porphyrin plane (Table 2). The ruthenium porphyrin is essentially planar (σ 0.046 Å). In addition, the *meso*-phenyl substituents on the ***p*-Ni-1** moiety are tilted further from orthogonality in **[*p*-Ni-1/tbRu-4/*p*-Ni-1]** (69.9° and 66.4°) than those in ***m*-Ni-1** (81.4° and 83.8°). The geometrical parameters of the ruthenium coordination sphere (Table 2) match well with those of the model complex $(DPAP)_2$**tbRu-4**; the Ru−P bond distance of 2.343(2) Å and the angle of the Ru−P bond to the porphyrin plane α 86.2° differ only slightly from those in $(DPAP)_2$**tbRu-4** (2.3623(10) Å, 89.5°).[19] Thus, attachment of the nickel porphyrin on the phosphine ligand does not significantly alter the coordination behavior of the phosphorus. The overall conformation of the complex is such that the two nickel(II) porphyrins are twisted in opposite directions with respect to the **tbRu-4** moiety, forming dihedral angles of 79.8° between the least-squares planes of the porphyrins. This conformation might be related to one of the conformations observed in the ^1H NMR spectra.

In the case of the rhodium porphyrins, the iodide is readily displaced upon mixing 2 equiv of the donor porphyrins with the acceptor porphyrin. The arrays adopt several geometries in solution that can be detected in the ^1H NMR spectra. For the β-pyrrole protons of **Rh-6**, three singlets at δ 9.01, 9.00, and 8.87 ppm could be found; also, the phosphine−phenyl proton resonances appear as two distinctively different sets of signals. For all rhodium-containing arrays, the ^{31}P NMR spectra only showed the characteristic doublet resonances ($\delta \sim -10$ ppm, $^1J_{Rh-P} \sim 90$ Hz) for the bisphosphine complexes with rhodium and no indication of the presence of various geometries, as in the ruthenium porphyrin arrays.

The three porphyrin arrays of the composition **D**−**A**−**D** can also be synthesized.[19,21] The arrays are stable in solution, judged from the ^1H and ^{31}P NMR spectra, and the phosphines are fully coordinated to the acceptor porphyrin in the millimolar concentration range. The rhodium arrays generally are easier to synthesize and show a better solubility in $CHCl_3$ than the ruthenium arrays. However, solubility is also greatly influenced by the nature of the acceptor porphyrin, which is enhanced for **Ru/Rh-4** and **Ru/Rh-6** but rather low for **Ru-3** and **Ru-5**.

The building blocks ***m*-2** allow us to build three porphyrin arrays where the acceptor porphyrins are located at the periphery. The order of the porphyrins is reversed, giving arrays of the form **A**−**D**−**A**. In Figure 9, the NMR spectra of the arrays **[Ru-4/*m*-Fb-2/Ru-4]** and **[Rh-5Me/*m*-Zn-2/Rh-5Me]** are displayed as representative examples. In the case of the ruthenium-containing arrays, three different species could be detected, which is best seen in the spectrum of **[Ru-4/*m*-Fb-2/Ru-4]**. The relative ratio of the signals at δ 8.96, 8.88, and 8.82 ppm is 0.2:1:0.8, an almost identical distribution to that in the array **[*m*-Fb-1/Ru-6/*m*-Fb-1]**. A close inspection of the ^1H NMR spectrum shows that for the meso protons of the **Ru-4** residue three large singlets and several small peaks can be observed; the meso protons of the ***m*-Fb-1** residue display at least four signals, and the signal for the pyrrole NH's at δ −2.43 ppm shows a much more complex pattern with several overlapped and broadened peaks (inset in Figure 9). This suggests that there could be an even larger diversity in conformations than expected. The ^{31}P NMR spectra show the phosphine resonances in the

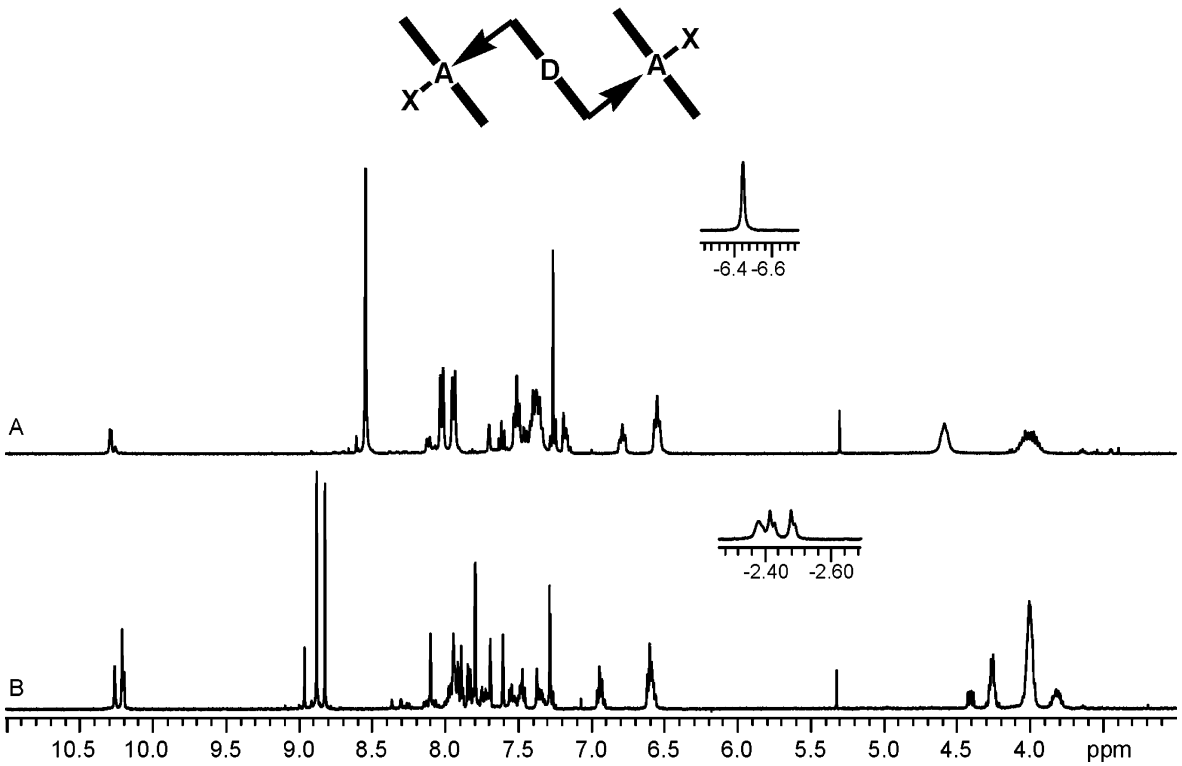

Figure 9. ^{1}H NMR spectra of (A) **[Rh-5Me/*m*-Zn-2/Rh-5Me]** (A−X = Rh-Me, D = Zn) and (B) **[Ru-4/*m*-Fb-2/Ru-4]** (A−X = Ru−CO, D = 2H). The inset in A shows the resonance of the rhodium bound methylide, and the inset in B displays the resonances of the pyrrole N−H's.

expected regions for monophosphine complexes. In the case of the ruthenium−porphyrin arrays, the ^{31}P NMR spectrum shows two signals, e.g., for **[Ru-6/*m*-Fb-2/Ru-6]** at δ −10.6 and −10.7 ppm. This was not observed for the **D**−**A**−**D** arrays. For the **[Rh-5Me/*m*-Zn-2/Rh-5Me]** complex, the phosphorus resonance is broadened and appears at a slightly lower field than the free phosphine, which is consistent with the observations made with DPAP and **Rh-5Me**.[21] No free phosphine could be detected in any case.

In summary, both mono- and disubstituted porphyrins ***m*/*p*-1** and ***m*-2** form stable complexes with both ruthenium and rhodium porphyrins. The composition of the arrays, **D**−**A**, **D**−**A**−**D**, or **A**−**D**−**A**, can be chosen by mixing the appropriate amounts of the building blocks in solution. The substitution pattern or the metalation state has no influence on the coordination ability of the phosphine, and in ***m*-2**, both phosphines are available for complexation. It should therefore be possible to form larger arrays, incorporating different porphyrins in the center and on the periphery. The arrays are not kinetically inert, judged from our studies with the model ligand DPAP;[19,21] this feature is in fact exploited to form dynamic combinatorial libraries.[16] For the trimeric arrays, this does however prevent the formation of arrays with different building blocks **A** and **A′** (or **D** and **D′**). Synthesizing mixed arrays of the form **A**−**D**−**A′** would result in scrambling and in the formation of a statistical mixture, composed of the three complexes **A**−**D**−**A**, **A′**−**D**−**A′**, and **A**−**D**−**A′**. No attempts were thus made to construct such mixed arrays. As we will show below, mixing different building blocks is still possible to a certain extent in larger arrays.

Assembly of Larger Arrays. The diphosphine-substituted porphyrin ***m*-2** and the bisphosphine complexes (P)Ru(P) or (P)Rh(P) can be regarded as chain extenders and the monophosphines ***m*/*p*-1**, (P)Ru(CO), and **(P)Rh-5Me** as chain terminators. Larger porphyrin arrays thus seem to be accessible by mixing appropriate equivalents of chain extender and chain terminator. The composition of these arrays would be either of the form **A**−**D**−(**A′**−**D**)$_n$−**A** or of the form **D**−**A**−(**D′**−**A**)$_n$−**D**. We therefore attempted to assemble larger arrays from different building blocks, incorporating structurally very different porphyrins into the complexes. For example, a 2:2:1 (**A**−**D**−**A′** or **D**−**A**−**D′**) mixture of ***m*-Fb-1**, **Rh-5**, and ***m*-Zn-2** or of **Ru-3**, ***m*-Fb-2**, and **Rh-5** should form arrays of the composition **[*m*-Fb-1/Rh-5/*m*-Zn-2/Rh-5/*m*-Fb-1]** or **[Ru-3/*m*-Fb-2/Rh-5/*m*-Fb-2/Ru-3]**, respectively. The complexities of both the ^{31}P NMR and ^{1}H NMR spectra increase as expected. The ^{31}P NMR spectrum of the latter mixture shows the two types of phosphine complexes: two doublets at $\delta \sim -10$ ppm for the rhodium bisphosphine in the center, and the broadened singlet at δ −15 ppm of the ruthenium monophosphine complex at the periphery of the array (see electronic SI for NMR spectroscopic details).

Changing the stoichiometry of the building blocks to 2:3:2 would yield seven porphyrin arrays of the composition **D**−**A**−**D′**−**A**−**D′**−**A**−**D**, e.g., **[*m*-Fb-1/Rh-5/*m*-Fb-2/Rh-5/*m*-Fb-2/Rh-5/*m*-Fb-1]** and **[*p*-Fb-1/Rh-4/*m*-Zn-2/Rh-4/*m*-Zn-2/Rh-4/*p*-Fb-1]**. The ^{31}P NMR spectrum showed several doublets at $\delta \sim -9$ ppm ($^1J_{\mathrm{Rh-P}} = 89$ Hz), consistent with the formation of bisphosphine complexes. Multiple singlets for the *meso*- and β-pyrrole protons show again an

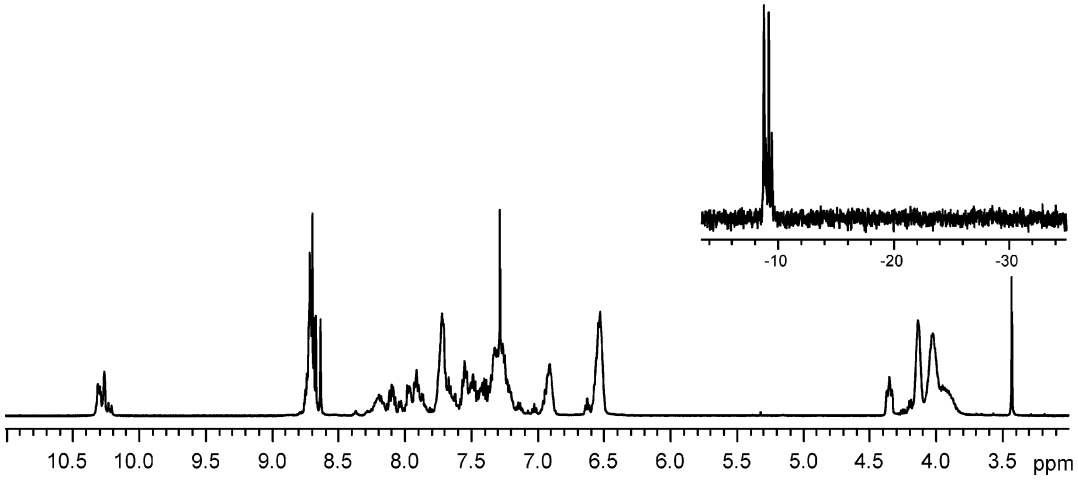

Figure 10. ^{1}H NMR spectrum of a 2:4:3 mixture of ***m*-Fb-1**, **Rh-5**, and ***m*-Zn-2**. The inset displays part of the ^{31}P NMR spectrum.

Scheme 2

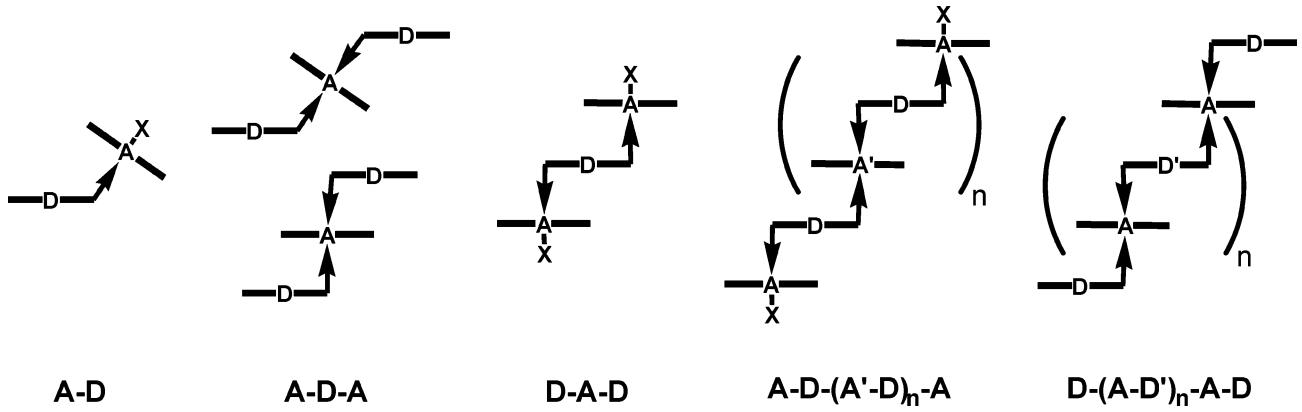

increased number of different complexes present. The 2:4:3 mixture of ***m*-Fb-1**, **Rh-5**, and ***m*-Zn-2** could yield a nine-porphyrin array **[*m*-Fb-1/Rh-5/*m*-Zn-2/Rh-5/*m*-Zn-2/Rh-5/*m*-Zn-2/Rh-5/*m*-Fb-1]**, of which both ^{1}H NMR and ^{31}P NMR spectra are displayed in Figure 10. No free phosphine is detectable in the ^{31}P NMR spectrum at δ −32 ppm; thus all the binding sites on rhodium are occupied by phosphine ligands.

One has to be cautious when analyzing higher-order architectures such as those described here because the kinetic lability leads to a weighted distribution of dimeric, trimeric, and higher-order assemblies, as can be observed in self-assembled supramolecular structures in solution.[25,26] The kinetic lability of the systems[16] unfortunately prohibits analysis of a molecular weight distribution using chromatographic methods, such as gel permeation chromatography or using mass spectrometry,[27] and the determination of the mole fractions of the individual complexes is not possible from the NMR spectroscopic data. Therefore, the complex mixtures described here may not contain the anticipated array as a major component. Nevertheless, any array formed will have the desired peripheral and central porphyrins incorporated as predetermined by the structure of the building blocks and by the relative stoichiometries in the mixtures.

Conclusions

We have demonstrated that phosphine-substituted porphyrins are versatile building blocks for the construction of supramolecular arrays. Arrays have been made incorporating three different porphyrins, as outlined in Scheme 2. The substitution pattern (meta or para) and the metalation state (free-base, zinc, nickel) has no influence on the affinity of the phosphine toward a variety of ruthenium and rhodium porphyrins. As for the acceptor porphyrins, variations in the porphyrin substituents, on both the *meso*- and β-pyrrole position, have no influence on the coordination as well. Even the bulky porphyrin **6** forms stable arrays with all phosphine porphyrins. The arrays are easily accessible simply by mixing appropriate amounts of the building blocks in solution. However, care has to be taken by choosing the correct acceptor porphyrins, i.e., if a rhodium porphyrin is intended to be located at the periphery. Also, if monophosphine ruthenium complexes are prepared, they cannot be isolated due to the lability of the bound carbonyl on ruthenium, which would be lost and result in scrambling of the array. By the introduction of a variety of different metalation states and substitution patterns, it should thus be possible to create arrays with well-defined electronic gradients, which could

(25) Ercolani, G. *Chem. Commun.* **2001**, 1416−1417.
(26) Ercolani, G. *J. Phys. Chem. B* **2003,** *107,* 5052−5057.
(27) Stulz, E.; Mak, C. C.; Sanders, J. K. M. *J. Chem. Soc., Dalton Trans.* **2001**, 604.

be used to transmit energy from either the periphery to the center, or vice versa. These interactions could be controlled by careful choice of the chain extenders and terminators.

Acknowledgment. We thank Brian Crysell, Duncan Howe, and Andrew Mason for help and support in running the NMR spectrometers. Financial support from the Swiss National Science Foundation (E.S.) and from the EPSRC is gratefully acknowledged. We thank a referee for helpful comments on the composition of the higher-order complexes.

Supporting Information Available: Full experimental details and analytical data of the building blocks, of the discussed arrays, and X-ray crystallographic files for ***m*-Fb-1**, ***m*-Zn-1**, ***m*-Ni-1**, and **[*p*-Ni-1/tbRu-4/*p*-Ni-1]** in PDF and CIF formats. This material is available free of charge via the Internet at http://pubs.acs.org.

IC034699W